FEBS Letters 586 (2012) 3452–3457

FEBS Letters

journal homepage: www.FEBSLetters.org

Structure of the GcpE (IspG)–MEcPP complex from *Thermus thermophilus*

Ingo Rekittke [a], Hassan Jomaa [a,*], Ulrich Ermler [b,*]

[a] Institut für Klinische Immunologie und Transfusionsmedizin, Justus-Liebig-Universität Giessen, Langhansstraße 7, 35392 Giessen, Germany
[b] Max-Planck-Institut für Biophysik, Max-von-Laue-Straße 3, D-60438 Frankfurt am Main, Germany

ARTICLE INFO

Article history:
Received 21 June 2012
Revised 24 July 2012
Accepted 27 July 2012
Available online 9 August 2012

Edited by Stuart Ferguson

Keywords:
Isoprenoid biosynthesis
GcpE
Iron–sulfur cluster
X-ray structure
Drug design

ABSTRACT

Isoprenoid precursor biosynthesis occurs through the mevalonate or the methylerythritol phosphate (MEP) pathway, used i.e., by humans and by many human pathogens, respectively. In the MEP pathway, 2-C-methyl-D-erythritol-2,4-cyclo-diphosphate (MEcPP) is converted to (*E*)-1-hydroxy-2-methyl-but-2-enyl-4-diphosphate (HMBPP) by the iron–sulfur cluster enzyme HMBPP synthase (GcpE). The presented X-ray structure of the GcpE–MEcPP complex from *Thermus thermophilus* at 1.55 Å resolution provides valuable information about the catalytic mechanism and for rational inhibitor design. MEcPP binding inside the TIM-barrel funnel induces a 60° rotation of the [4Fe–4S] cluster containing domain onto the TIM-barrel entrance. The apical iron of the [4Fe–4S] cluster ligates with the C3 oxygen atom of MEcPP.

1. Introduction

Isoprenoids – vital for all organisms – represent a large family (>55 000) of compounds including i.e., dolichol, quinones, carotenoids and sterols [1]. All isoprenoids are derived from two universal precursors – isopentenyl diphosphate and dimethylallyl diphosphate – that are biosynthesized in nature by two different pathways. The well-established mevalonate pathway is used by animals, fungi, archaea and some bacteria and the more recently discovered 2-C-methyl-D-erythritol-4-phosphate (MEP) pathway (Fig. 1) by most bacteria and parasitic protozoa of the phylum apicomplexa [2–4]. Plants utilize both pathways, the mevalonate pathway in the cytosol and the MEP pathway in the plastids. Since humans exclusively use the mevalonate pathway, the enzymes of MEP pathway are attractive targets for the development of antimicrobial and herbicidal drugs [2,5].

The penultimate step of the MEP pathway is the conversion of 2-C-methyl-D-erythritol-2,4-cyclo-diphosphate (MEcPP) into (*E*)-1-hydroxy-2-methyl-but-2-enyl-4-diphosphate (HMBPP) by the HMBPP synthase, termed GcpE or IspG (Fig. 1). The [4Fe–4S] cluster containing enzyme GcpE occurs in two variants distinguished by a molecular mass of ca. 44 and 79 kDa, respectively [6–10]. The physiological electron donor for reducing the iron–sulfur cluster appears to be either a ferredoxin or a flavodoxin depending on the organism [11,12]. Dithionite and/or 5-deazaflavin are frequently used as electron donor for *in vitro* studies [7,8,10]. Various mechanistic proposals involving cationic, radical, anionic, epoxide and ferraoxetane intermediates for the reductive ring-opening reaction have been reported mainly based on EPR and NMR spectroscopic studies [13–16]. The catalytic mechanism appears to be similar in both GcpE variants [17]. X-ray structures of GcpE from *Aquifex aeolicus* and *Thermus thermophilus* published recently [18,19] revealed for the first variant a homodimeric enzyme with each monomer being composed of two spatially separated domains connected by a solvent-exposed linker of five amino acids (286–290) (Fig. 2A, Supplementary Fig. 1). The TIM-barrel domain (4–285) consists of a canonical $(\beta\alpha)_8$ barrel (β1–8, α1–8) enlarged by a N-terminal β-hairpin located at the barrel bottom and a helix-loop-helix protrusion after strand 5. It was assumed that the substrate binding site is situated inside a funnel-shaped pocket created at the C-terminal side of the eight parallel β-strands. The C-terminally fused α/β-domain consists of a five-stranded mixed β-sheet (β1′-5′) flanked by three helices (α1′-3′) that hosts the [4Fe–4S] cluster at the C-terminal strand end of the β2′α2′β3′ motif. Dimeric GcpE is built up by a head-to-tail arrangement of the two subunits such that the α/β-domain of one subunit is attached

Abbreviations: GcpE, (*E*)-1-hydroxy-2-methyl-but-2-enyl-4-diphosphate synthase; MEP, 2-C-methyl-D-erythritol-4-phosphate; MEcPP, 2-C-methyl-D-erythritol-24-cyclo-diphosphate; HMBPP, (*E*)-1-hydroxy-2-methyl-but-2-enyl-4-diphosphate

* Corresponding author. Fax: +49 641 985 41509 (H. Jomaa), fax: +49 69 6303 1002 (U. Ermler).
E-mail addresses: hassan.jomaa@uniklinikum-giessen.de (H. Jomaa), ulrich.ermler@biophys.mpg.de (U. Ermler).

0014-5793/$36.00
http://dx.doi.org/10.1016/j.febslet.2012.07.070

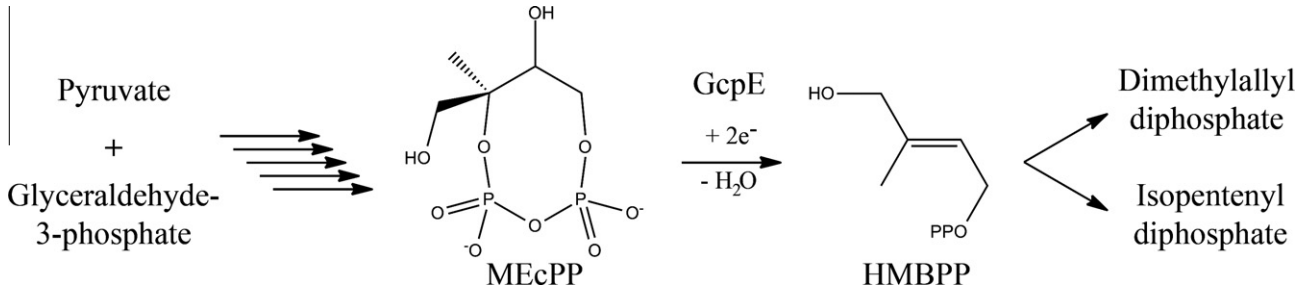

Fig. 1. Reaction of GcpE. GcpE catalyzes the penultimate step of the MEP pathway by converting MEcPP into HMBPP.

to the TIM-barrel domain of the counter one and vice versa [18,19]. In addition, the two TIM-barrel domains form an extended interface and are therefore considered as the rigid core of GcpE (Fig. 2A).

To establish the structural basis for understanding the GcpE reaction and for the design of knowledge-based inhibitors we solved the X-ray structure of the *T. thermophilus* GcpE–MEcPP complex at 1.55 Å resolution. We describe the conformation of the complex in a closed state, the binding mode of the substrate and discuss the mechanistic implications of the structural results.

2. Materials and methods

2.1. Enzyme production

Cloning, expression and purification of GcpE of *T. thermophilus* were described in detail [7,19]. Briefly, the PQETtGcpE vector, containing untagged GcpE, was transformed into TOP10 *E. coli* cells (Invitrogen). Cell cultivation was performed in LB broth medium (Roth) supplemented with 150 μg ml^{-1} ampicilin and 300 μM $FeCl_3$ at 37 °C. DEAE, Source 15Q and Superdex200 columns were applied for purification. GcpE was stored at a concentration of ca. 10 mg ml^{-1} in 30 mM Tris–HCl, pH 7.5 and 150 mM NaCl. All experimental steps after cell cultivation were carried out under oxygen exclusion.

2.2. Crystallization and X-ray structure analysis

Crystallization screens were performed at 18 °C using the sitting drop vapor diffusion method combined with the random microseeding [20], thereby utilizing GcpE-crystals grown in 30% (v/v) MPD and 20% (v/v) ethanol (sitting drop) for seed production [21]. Best diffracting crystals grew in 0.6 μl enzyme solution, containing 5 mM MEcPP, and 0.6 μl precipitant composed of 45% pentaerythritol propoxylate 426, 0.1 M MES pH 6.0, 0.4 M KCl, 0.1% NaN_3 (JBScreen Pentaerythritol 1, C6, Jena Bioscience) and 0.1 μl seed stock. Data were collected at the Swiss-Light source beamline PXII and processed with XDS [22]. Phases were determined by PHASER [23] using the TIM-barrel and α/β-domains as separated search models. The structure was refined using REFMAC [24] and PHENIX [25]. Crystal parameters, data collection and refinement statistics are listed in Supplementary Table 1. Figs. 2–5 were produced with PYMOL (Schrödinger, LLC). The atomic coordinates and structure factors of GcpE–MEcPP have been deposited in the Protein Data Bank, www.pdb.org with ID code 4G9P.

3. Results and discussion

3.1. Global structural differences between the GcpE–MEcPP and GcpE structures

Recombinant untagged *T. thermophilus* GcpE was crystallized in presence of 5 mM MEcPP under strictly anaerobic conditions; the resulting X-ray structure was refined to R/R_{free}-factors of 17.7/20.3% at 1.55 Å resolution (Supplementary Table 1). The asymmetric unit contains one monomer and the functional homodimer is built up by a crystallographic twofold axis present in the space group $P6_522$.

The GcpE–MEcPP complex and (substrate-free) GcpE structures are distinguished by a large-scale rearrangement of the two α/β-domains relative to the two TIM-barrel core (Fig. 2) which turned the homodimeric enzyme from an open and rather mobile into a closed and compact form. The rotation angle is ca. 60° (to open *A .aeolicus* GcpE ca. 50° [18]) considering the TIM-barrel core as fixed reference point. Ala289, a residue of the interdomain linker, serves as the hinge point. In this open-to-closed process already predicted [18,19] and very recently substantiated [17], the α/β-domain parked on the helix-loop-helix protrusion in the open GcpE structure swings from its edge towards the entrance of the counter

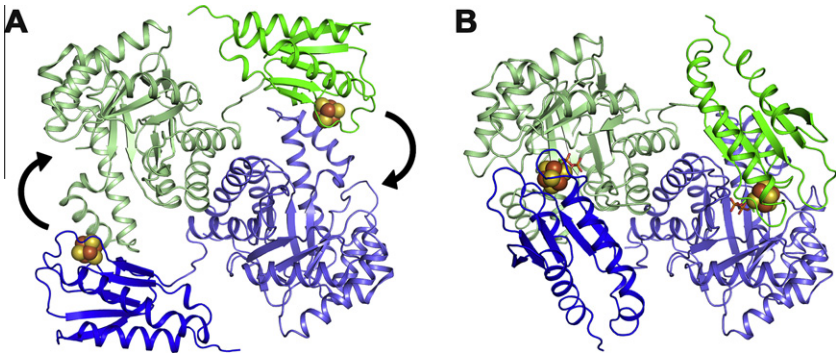

Fig. 2. Open-to-closed transition: (A) GcpE structure without substrate. The active site is formed between the TIM-barrel domain (lightgreen, blue) of one subunit and the α/β-domain of the counter subunit (lightblue, green). The [4Fe–4S] cluster of the α/β-domain is ca. 25 Å apart from the active site. An extended contact area is formed between helices 6, 7 and 8 of the TIM-barrel domains of both subunits. (B) The MEcPP–GcpE structure. The α/β-domain is rotated ca. 60° from the helix-loop-helix protrusion towards the funnel entrance of the TIM-barrel and locks the MEcPP binding site.

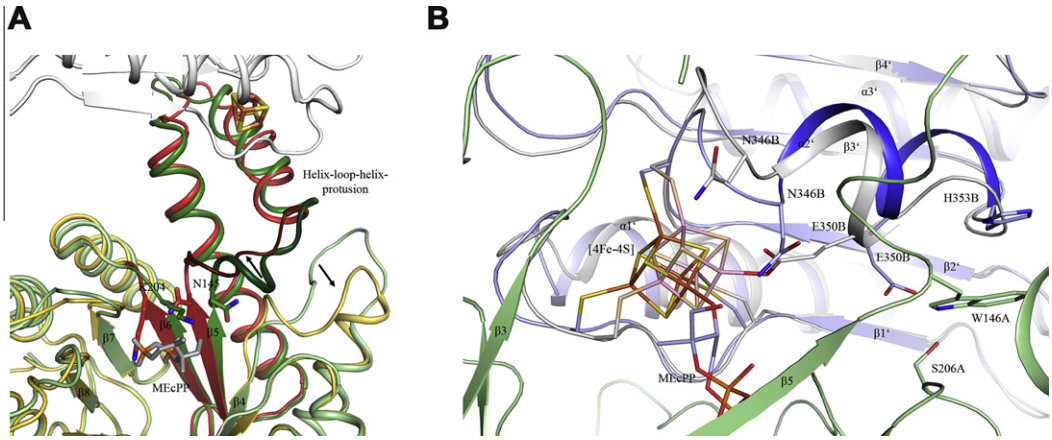

Fig. 3. MEcPP-induced rearrangement of the α/β-domain. (A) Superposition of the TIM-barrel domain of the GcpE (yellow) and GcpE–MEcPP (lightgreen) structures. The α/β-domain in the open state is shown in grey. Substrate binding is conformationally propagated to strands 5 and 6 and from there to the helix-loop-helix protrusion highlighted in red/green. The loops following strands 4 and 5 are marked by an arrow. (B) Superposition of the α/β-domains in the closed (light-blue) and open (grey) states. In the closed state the position of the ISC crevice and the [4Fe–4S] cluster therein is fine-tuned to form a covalent bond to the substrate and to optimize the new interactions to the TIM-barrel domain (lightgreen). Helix 2′ in the closed state is drawn in blue emphasizing its substantial positional change.

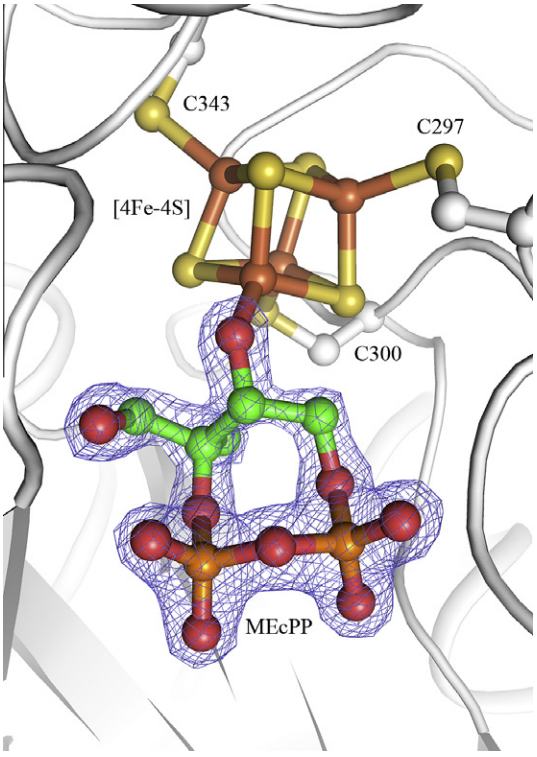

Fig. 4. [4Fe–4S] cluster and MEcPP binding. The 1.55 Å F_{obs}–F_{calc} omit electron density (blue) drawn at a contour level of 4σ indicate the conformation of MEcPP and the covalent bond between the [4Fe–4S] cluster and MEcPP.

TIM-barrel funnel in the closed GcpE–MEcPP structure. Strand 1′ and helix 2′ are detached from the helix-loop-helix protrusion (contact area ca. 460 Å^2) and form a new extended interface (ca. 2350 Å^2) built up mainly by helices 1′ and 2′, strand 1′and the following loop of the α/β-domain and the C-terminal loops of each TIM-barrel strand (except for the one following strand 4). The interactions are characterized by a comparatively small number of direct hydrogen bonds but by multiple van der Waals and solvent mediated contacts. This type of interaction suggests a small binding affinity relative to the large contact area which is comprehensible in order to fix the α/β-domain in a specific conformation on one hand but to allow its release after product formation on the other. After locking the funnel-shaped pocket of the TIM-barrel by the displaced α/β-domain, a cavity is created that largely shields the substrate binding site from bulk solvent (Fig. 2).

Although domain rearrangement and substrate binding (see below) has kept the overall fold of the individual domains unchanged reflected in rms deviations of 1.4 Å (1.7 Å to GcpE of *A. aeolicus*) for the TIM-barrel and 1.3 Å (2.5 Å) for the α/β-domains significant conformational differences within the two domains become visible upon separated superposition [26] (Fig. 3). The TIM-barrel domains are distinguished by a concerted twist of the C-terminal ends of strands 4–7 within the barrel wall of 2.0–3.0 Å. The loop after strand 5 and the following helix and loop of the helix-loop-helix protrusion are slightly rotated resulting in a shift at its edge up to 3.7 Å. In addition, the loop following strand 4 that underpins the helix-loop-helix protrusion in the open state moves up to 10 Å from a highly solvent-exposed position towards the barrel center in the closed state (Fig. 3A). Structural differences between the α/-domains in the open and closed state especially include the C-terminal end of strands β1′ and β2′, the following loops and helix α2′ which constitute the iron–sulfur cluster binding crevice abbreviated as ISC crevice (Fig. 3B). The conformational changes in the range of 2.5–3.5 Å are complex in order to account for the distinct interface with the TIM-barrel and the slightly shifted position of the [4Fe–4S] cluster (see below) in the open and closed states. For example, Thr303 interacting with S4 of the [4Fe–4S] cluster in both states moves ca. 1.8 Å but the following residue Thr304 ca. 5 Å to avoid a collision with the TIM-barrel (Supplementary Fig. 2).

3.2. [4Fe–4S] binding

The GcpE–MEcPP structure revealed a completely occupied [4Fe–4S] cluster with a homogeneous Fe content reflected in temperature factors of 13.6 ± 0.6 Å^2 (Fig. 4). Due to the described rigid-body movement of the α/β-domain the [4Fe–4S] cluster is displaced ca. 25 Å and points from the center of the TIM-barrel entrance towards the bottom of the created cavity occupied by the substrate (Fig. 2). The [4Fe–4S] cluster thereby remains embedded in the ISC crevice but becomes capped essentially by the substrate and not anymore by the helix-loop-helix protrusion. (The interactions between the [4Fe–4S] cluster and the TIM-barrel domain are limited to Met158 in the open state and Thr58 and Asp87 mediated

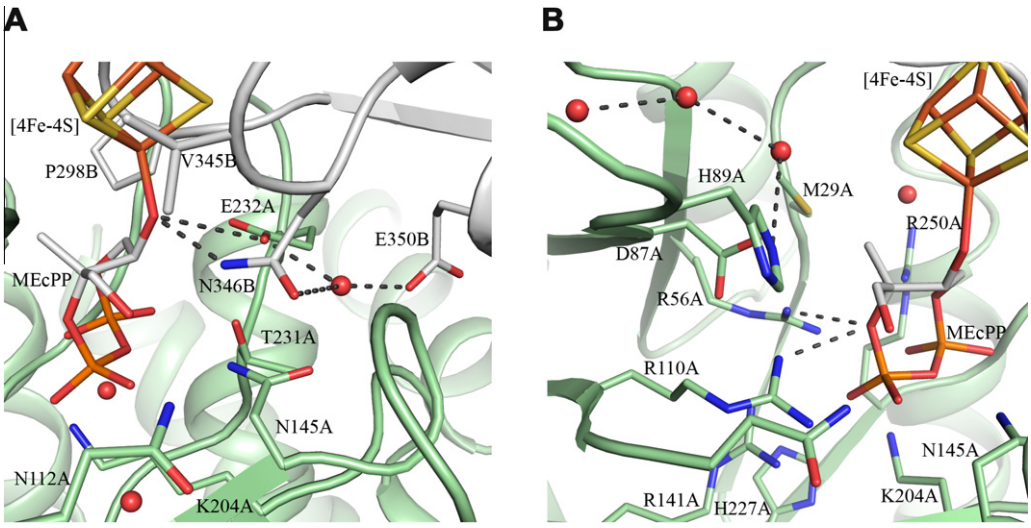

Fig. 5. Active site architecture and proton transfer routes. (A) Region around Glu232 that is potentially involved in the deprotonation of the C3 hydroxyl group during formation of the covalent bond to the [4Fe–4S] cluster. The TIM barrel domain is colored in lightgreen, the α,β domain in grey and solvent molecules as red spheres. (B) Region around the bond between C2 and the β-phosphate oxygen that has to be cleaved during the reaction and around the Asp87-His89 pair that is possibly involved in protonating the oxygen being dissociated as H_2O.

by a solvent molecule in the closed state.) Three of the four irons are ligated with Cys297, Cys300 and Cys343 and most non-covalent contacts between the [4Fe–4S] cluster and the α/β-domain are unchanged in the open and closed states. However, the fourth iron that coordinates to Glu350 in the open state is ligated to the C3 oxygen of MEcPP in the closed state (Fig. 4).

Due to the complex conformational change of the ISC crevice upon open-to-closed transition, the crevice becomes slightly widened and the [4Fe–4S] cluster displaced (Fig. 3B). Thus, the iron–sulfur cluster becomes better accessible for the substrate which is crucial for forming a strong bond. The small displacement of the [4Fe–4S] cluster, in particular, of the apical iron of 1.7 Å is mainly caused by Cys300 that is shifted nearly 3 Å and contacts the C-terminal side of strand 1 of the counter TIM barrel (Fig. 3B). Moreover, helix 2′ is slightly tilted parallel to the β-sheet plane of the α/β-domain, Glu350 becomes thus sequestered and its side chain swings away from the [4Fe–4S] cluster towards the TIM-barrel thereby forming a hydrogen bond with Trp146 and Ser206. The distance between the carboxylate group of Glu350 in the closed and open states is more than 6.5 Å. Asn346 of helix 2′ in contact to S3 of the [4Fe–4S] cluster and to Asp159 in the open state partly occupies the place of the displaced Glu350 in the closed state (Fig. 3B). In this position, Asn346 multiply interacts with the loop following strand 5 (hydrogen bonded with Ser148) of the TIM-barrel, is 4.1 Å apart from the apical iron and contacts the substrate (see below).

3.3. Substrate binding

As already predicted from structural studies of the open state [18,19], the substrate MEcPP is accommodated in the cavity located between the C-terminal side of the TIM-barrel and the counter α/β-domain (acting as lid) (Fig. 2). The occupancy of the substrate was refined to nearly 100% and the temperature factors to 13.6 ± 1.7 Å ^{2} suggesting a highly rigid binding mode for MEcPP. MEcPP was found in a boat-shaped conformation with the methylerythritol and pyrophosphate parts at the top and the linking oxygens bound to the C2 and C4 atoms at the bottom. The excellent electron density of 1.55 Å resolution clearly confirms the previously determined *S* and *R* configuration of the asymmetric C2 and C3 atoms [6] (Fig. 4) .

MEcPP is oriented in a manner that the methylerythritol part points to the α/β-domain thereby facing the [4Fe–4S] cluster and the diphosphate part is directed to the pocket bottom (Fig. 5). MEcPP forms a series of interactions to the polypeptide illustrated in Supplementary Fig. 3. In particular, the diphosphate part is multiply hydrogen bonded to side chains of conserved acidic residues as Arg56, Arg110, Arg141, Arg260 and Lys204 (Fig. 5). The C1-hydroxyl substituent is in van der Waals contact to Asp87, His89, Arg110 and Asn112, however, the distances of 3.5–4 Å suggest rather weak interactions (Fig. 5B). The catalytically crucial C2, C3 and C3 oxygen atoms of the erythritol part contact the [4Fe–4S] cluster, Met29, Pro298, Val345 and Asn346. As mentioned, the C3 oxygen dissociated during the chemical reaction (Fig. 1) is ligated to the apical iron of the [4Fe–4S]-cluster and hydrogen bonded to Asn346 of the counter α/β-domain (Fig. 5A). The established molecular basis of substrate binding offers a rational platform for designing inhibitors for GcpE.

Comparison between the GcpE–MEcPP and GcpE structures reveals an induced-fit process upon substrate binding with larger side chain rearrangements of Asn112, Asn145, Lys204, Thr231 and Glu232 that optimize hydrogen bond interactions to MEcPP. The importance of the invariant Asn145 and Glu232 was already verified by site-directed mutagenesis studies on the *A. aeolicus* enzyme [18].

3.4. Mechanism

Despite various proposals the complex mechanism of the reductive deoxygenase reaction from MEcPP to HMBPP is not sufficiently understood [13–15]. The presented structure of the GcpE–MEcPP complex does not directly contribute to the elucidation of the chemical nature of the involved short-living intermediates but provide information about dynamic aspects of the reaction and about geometrical restraints that should be integrated into further mechanistic considerations. Pronounced active site features and their implications for catalysis are summarized under items 1–7. From this perspective we proposed an enzymatic mechanism (Supplementary Fig. 4).

(1) The predicted large-scale open-to-closed transition upon substrate binding [18,19], indeed, exists and builds up the active site architecture prior to the reaction (Fig. 2). An open

state is indispensable as MEcPP is too bulky for entering the pocket in the closed state. Although the [4Fe–4S] cluster is buried an external electron donor i.e., ferredoxin can be placed sufficiently close to ensure effective electron transfer in the closed state.

(2) The structural data offer a convincing picture regarding the substrate-induced rearrangement of the α/β-domain relative to the TIM-barrel core. Accordingly, side chains of the TIM-barrel funnel, in particular, Asn145 and Lys204 of strands 5 and 6 are attracted by the incoming substrate and change their conformation to adjust an optimal hydrogen-bond with the pyrophosphate of MEcPP (Fig. 3A). The thereby induced concerted twist at the C-terminal end of strands 4–7 is directly propagated via strand 5 to the helix-loop-helix protrusion. Its small rotation implicates one collision (Thr155-Oγ-Cys300-O 1.9 Å) and a decreased number of van der Waals contacts to the α/β-domain in the open state and eventually induces its detachment. Notably, the loop after strand 5 undergoes a structural rearrangement up to 5 Å and builds up the interface to the α/β-domain in the closed state (Fig. 3A). Interdomain interactions, in particular, those between this loop and helix 2′ as well as loops after strands 1 + 2 and the loop after strand 1′ might trigger the conformational changes within the ISC crevice when the arriving α/β-domain reaches its binding site (Fig. 3B). Accompanied by this "lock into place" process Glu350 is pulled away from the [4Fe–4S] cluster and becomes fixed by hydrogen-bonds to Ser206 and Trp146. The C3 oxygen of MEcPP occupies its fourth iron ligation site of the closed state. Interestingly, the indol group of Trp146 (of the loop after strand 5) contacts Pro298 of the counter α/β-domain in the open state. Upon substrate binding Trp146 changes its conformation by nearly 10 Å, collide with the helix-loop-helix protrusion via His171 in the open state (thereby promoting the open-to-close transition) and interacts again with the α/β-domain in the closed state. As the postulated MEcPP induced-fit process is initiated by protein-MEcPP interactions, a modified position of the product HMBPP might impair the described interactions and the enzyme returns into the open state.

(3) The apical Fe of the [4Fe–4S] cluster definitively forms a covalent bond to the C3 oxygen of MEcPP already deduced from spectroscopic data [14,15,27]. Their distance is 1.8 Å and the angle between atoms Fe1, the C3 oxygen and C3 is 124° (Fig. 4). No evidence for epoxide formation prior to reduction were detectable in the electron density map implicating that the open-to-closed transition can be triggered by MEcPP. Crystallization was performed in a 95% N_2/5% H_2 atmosphere without adding further reducing agents.

(4) Covalent bond formation implies deprotonation of the C3 hydroxyl group of MEcPP that might be assisted by Asn346 and Glu232. Glu232 might act as proton acceptor, although its distance of 3.8 Å to the hydroxyl group is rather long (Fig. 5A). The basicity of the carboxylate group of Glu232 is increased by a solvent-mediated contact to Asn346 and Glu350 the latter being directly accessible to bulk solvent. Thus, Glu350 appears to have a dual function, first, as ligand of the [4Fe–4S] cluster in the open state and second as part of a proton-relay system in the closed state (Fig. 3B). Site-specific mutations of Glu350 in the *A. aeolicus* enzyme exhibited a low enzymatic activity [18].

(5) Upon ring cleavage between atoms C2 and the β-phosphate oxygen of MEcPP, adjacent acidic residues (see Supplementary Fig. 2), in particular the invariant Arg56 and Arg110 increase the leaving group potential of the phospho group by compensating the generated negative charge (Fig. 5). Their exchange to lysine in the *A. aeolicus* enzyme result in a very low specific activity [18]. Protonation of the released phospho group by a firmly bound water molecule or via His227 hydrogen-bonded to Lys204 is, in principle, feasible.

(6) Ring cleavage requires a separation between atoms C2 and the β-phosphate oxygen of the substrate up to a distance of at least 3 Å. The pyrophosphate is wrapped so tightly by the protein matrix that essentially no obvious free space for movements exists. In contrast, C2 (and its methanol and methyl substituents) might evade the pyrophosphate towards and lateral to the [4Fe–4S] cluster and towards Asp87 (Fig. 5B).

(7) HMBPP formation requires the dissociation of the oxygen covalently bound either to atoms C2 or C3 of an intermediate species that becomes, at first, most likely protonated. The most suitable candidates for proton donation are Glu232 geometrically favored when the oxygen is bound to C3 and the Asp87-His89 pair when the oxygen is bound to C2 (Fig. 5). EPR spectroscopic data suggest a C3 rather than a C2 bound oxygen in an intermediate species [15,28], Mutational studies indicated a crucial function of the strictly conserved Asp87 [18]. The GcpE–MEcPP structure underscores the importance of Asp87 for catalysis as it is positioned at the terminal point of an uninterrupted water chain that extends to bulk solvent and might thus serve together with the invariant His89 as suitable proton source. Disregarding larger conformational changes, the distance of ca. 6 Å between Asp87 and the C3 bound oxygen species appears to be too long for a direct catalytic role. Further studies are necessary to clarify this uncertain point.

Acknowledgments

This work was supported by the Else Kröner-Fresenius-Stiftung and the Max-Planck Society. We thank Hartmut Michel for continuous support and Tobias Weinert and the staffs of PXII at the Swiss Light Source (Villigen) for help during data collection.

Appendix A. Supplementary data

Supplementary data associated with this article can be found, in the online version, at http://dx.doi.org/10.1016/j.febslet.2012.07.070.

References

[1] Sacchettini, J.C. and Poulter, C.D. (1997) Creating isoprenoid diversity. Science 277, 1788–1789.
[2] Grawert, T., Groll, M., Rohdich, F., Bacher, A. and Eisenreich, W. (2011) Biochemistry of the non-mevalonate isoprenoid pathway. Cell. Mol. Life Sci. 68, 3797–3814.
[3] Rohmer, M., Knani, M., Simonin, P., Sutter, B. and Sahm, H. (1993) Isoprenoid biosynthesis in bacteria: a novel pathway for the early steps leading to isopentenyl diphosphate. Biochem. J. 295 (Pt. 2), 517–524.
[4] Rohmer, M. (2008) From molecular fossils of bacterial hopanoids to the formation of isoprene units: discovery and elucidation of the methylerythritol phosphate pathway. Lipids 43, 1095–1107.
[5] Rohdich, F., Bacher, A. and Eisenreich, W. (2005) Isoprenoid biosynthetic pathways as anti-infective drug targets. Biochem. Soc. Trans. 33, 785–791.
[6] Hecht, S., Eisenreich, W., Adam, P., Amslinger, S., Kis, K., Bacher, A., Arigoni, D. and Rohdich, F. (2001) Studies on the nonmevalonate pathway to terpenes: the role of the GcpE (IspG) protein. Proc. Natl. Acad. Sci. U S A 98, 14837–14842.
[7] Kollas, A.K. et al. (2002) Functional characterization of GcpE, an essential enzyme of the non-mevalonate pathway of isoprenoid biosynthesis. FEBS Lett. 532, 432–436.
[8] Seemann, M., Bui, B.T., Wolff, M., Tritsch, D., Campos, N., Boronat, A., Marquet, A. and Rohmer, M. (2002) Isoprenoid biosynthesis through the methylerythritol phosphate pathway: the (*E*)-4-hydroxy-3-methylbut-2-enyl diphosphate synthase (GcpE) is a [4Fe–4S] protein. Angew. Chem., Int. Ed. 41, 4337–4339.

[9] Querol, J., Campos, N., Imperial, S., Boronat, A. and Rodriguez-Concepcion, M. (2002) Functional analysis of the Arabidopsis thaliana GCPE protein involved in plastid isoprenoid biosynthesis. FEBS Lett. 514, 343–346.
[10] Seemann, M., Wegner, P., Schunemann, V., Bui, B.T., Wolff, M., Marquet, A., Trautwein, A.X. and Rohmer, M. (2005) Isoprenoid biosynthesis in chloroplasts via the methylerythritol phosphate pathway: the (*E*)-4-hydroxy-3-methylbut-2-enyl diphosphate synthase (GcpE) from Arabidopsis thaliana is a [4Fe–4S] protein. J. Biol. Inorg. Chem. 10, 131–137.
[11] Zepeck, F., Grawert, T., Kaiser, J., Schramek, N., Eisenreich, W., Bacher, A. and Rohdich, F. (2005) Biosynthesis of isoprenoids. Purification and properties of IspG protein from *Escherichia coli*. J. Org. Chem. 70, 9168–9174.
[12] Seemann, M., Tse Sum Bui, B., Wolff, M., Miginiac-Maslow, M. and Rohmer, M. (2006) Isoprenoid biosynthesis in plant chloroplasts via the MEP pathway: direct thylakoid/ferredoxin-dependent photoreduction of GcpE/IspG. FEBS Lett. 580, 1547–1552.
[13] Rohdich, F. et al. (2003) The deoxyxylulose phosphate pathway of isoprenoid biosynthesis: studies on the mechanisms of the reactions catalyzed by IspG and IspH protein. Proc. Natl. Acad. Sci. U S A 100, 1586–1591.
[14] Wang, W., Li, J., Wang, K., Huang, C., Zhang, Y. and Oldfield, E. (2010) Organometallic mechanism of action and inhibition of the 4Fe–4S isoprenoid biosynthesis protein GcpE (IspG). Proc. Natl. Acad. Sci. U S A 107, 11189–11193.
[15] Xu, W., Lees, N.S., Adedeji, D., Wiesner, J., Jomaa, H., Hoffman, B.M. and Duin, E.C. (2010) Paramagnetic intermediates of (*E*)-4-hydroxy-3-methylbut-2-enyl diphosphate synthase (GcpE/IspG) under steady-state and pre-steady-state conditions. J. Am. Chem. Soc. 132, 14509–14520.
[16] Nyland 2nd, R.L., Xiao, Y., Liu, P. and Freel Meyers, C.L. (2009) IspG converts an epoxide substrate analogue to (*E*)-4-hydroxy-3-methylbut-2-enyl diphosphate: implications for IspG catalysis in isoprenoid biosynthesis. J. Am. Chem. Soc. 131, 17734–17735.
[17] Liu, Y.L. et al. (2012) Structure, function and inhibition of the two- and three-domain 4Fe–4S IspG proteins. Proc. Natl. Acad. Sci. U S A 109, 8558–8563.
[18] Lee, M., Grawert, T., Quitterer, F., Rohdich, F., Eppinger, J., Eisenreich, W., Bacher, A. and Groll, M. (2010) Biosynthesis of isoprenoids: crystal structure of the [4Fe–4S] cluster protein IspG. J. Mol. Biol. 404, 600–610.
[19] Rekittke, I., Nonaka, T., Wiesner, J., Demmer, U., Warkentin, E., Jomaa, H. and Ermler, U. (2011) Structure of the E-1-hydroxy-2-methyl-but-2-enyl-4-diphosphate synthase (GcpE) from *Thermus thermophilus*. FEBS Lett. 585, 447–451.
[20] D'Arcy, A., Villard, F. and Marsh, M. (2007) An automated microseed matrix-screening method for protein crystallization. Acta Crystallogr. D Biol. Crystallogr. 63, 550–554.
[21] Shaw Steward, P.D., Kolek, S.A., Briggs, R.A., Chayen, N.E. and Baldock, P.F.M. (2011) Random microseeding: a theoretical and practical exploration of seed stability and seeding techniques for successful protein crystallization. Cryst. Growth Des. 11, 3432–3441.
[22] Kabsch, W. (2010) Xds. Acta Crystallogr. D Biol Crystallogr. 66, 125–132.
[23] McCoy, A.J., Grosse-Kunstleve, R.W., Adams, P.D., Winn, M.D., Storoni, L.C. and Read, R.J. (2007) Phaser crystallographic software. J. Appl. Crystallogr. 40, 658–674.
[24] Murshudov, G.N., Vagin, A.A. and Dodson, E.J. (1997) Refinement of macromolecular structures by the maximum-likelihood method. Acta Crystallogr. D Biol. Crystallogr. 53, 240–255.
[25] Afonine, P.V. et al. (2010) Phenix.model_vs_data: a high-level tool for the calculation of crystallographic model and data statistics. J. Appl. Crystallogr. 43, 669–676.
[26] Holm, L. and Rosenstrom, P. (2010) Dali server: conservation mapping in 3D. Nucleic Acids Res. 38, W545–W559.
[27] Adedeji, D., Hernandez, H., Wiesner, J., Kohler, U., Jomaa, H. and Duin, E.C. (2007) Possible direct involvement of the active-site [4Fe–4S] cluster of the GcpE enzyme from *Thermus thermophilus* in the conversion of MEcPP. FEBS Lett. 581, 279–283.
[28] Wang, W., Wang, K., Li, J., Nellutla, S., Smirnova, T.I. and Oldfield, E. (2011) An ENDOR and HYSCORE investigation of a reaction intermediate in IspG (GcpE) catalysis. J. Am. Chem. Soc. 133, 8400–8403.